Resonant phenomena and mechanism in vibrated granular systems

Hui Cai [1,*] and Guoqing Miao[2]

[1]*School of Electrical Engineering, Yancheng Institute of Technology, Yancheng 224051, China*
[2]*Institute of Acoustics and Key Laboratory of Modern Acoustics of Ministry of Education, Nanjing University, Nanjing 210093, China*

We were motivated to perform this research by the investigation of Brownian motors in excited granular materials converting the chaotic motion of granules into the oriented motion of motors. We conducted experimental studies to explore the horizontal motion of granules in vertically vibrated annular granular systems, including mixed and pure granular systems with an asymmetrical periodic structure on the bottom. The variations of the horizontal granular flow caused by the height, vibrating parameters, and mixing ratio were described in detail. Our results revealed considerable changes in the horizontal flow of different granular systems. Most importantly, resonance was induced in the horizontal granular flow by the vertical vibration; that is, the horizontal flow reached its maximum at specific vibrating parameters. A collisional model of rigid objects was constructed to probe the flowing resonances in these granular systems and provided a qualitative agreement with the experimental results obtained. We conclude that when a flowing resonance occurs, the granular system oscillates horizontally with a natural frequency under periodic external excitation. The frequency matching between the external excitation and the horizontal oscillation is responsible for the flowing resonance. Our results could improve the current understanding of the dynamic properties of granular systems under external excitation.

I. INTRODUCTION

Resonant phenomena are widespread in nature and have been extensively studied and exploited in many scientific fields [1,2]. In classical mechanics, resonance is the mechanism due to which a pendulum acts [3,4], for example, playing on a swing. When a person on the swing is pushed with a frequency approaching the swing's natural frequency, the swing goes higher until it reaches maximum amplitude. This effect is caused by the resonance of the swing with pushes, resulting in the absorption of increasingly higher kinetic energy from pushes. In optics, the light and other short waves are generated by resonances on the atomic scale such as electrons transition in atoms. Resonances at the atomic scale are the basis of a number of spectroscopic techniques, such as nuclear magnetic resonance [5–7], which are widely used in condensed matter physics.

It is interesting and meaningful to explore the resonance in a noncohesive, strongly dissipative system, which is driven by external forces, such as a granular system under harmonic vertical vibration [8–12]. However, the corresponding investigation has not been substantially performed. The inelastic bouncing ball model revealed that the resonant phenomenon is a canonic characteristic of the nonlinear dynamics of bouncing bodies [13,14]; while no resonant phenomena have been reported when this approach was widely used to characterize the dynamics of vertically vibrated granular systems [15,16]. In Ref. [17], by analyzing the temporal dependencies of mean-squared velocity and height of the center of mass, a resonant effect was presented in the vertically vibrated granular system;

it was believed that such a resonant behavior induced granular segregation. In Ref. [18], the efficiency of energy transferal to a dense, vibrated granular bed was found to be influenced by the frequency of oscillations, which were used to drive the system, which demonstrated the existence of resonant behavior in the granular bed. In our study, we also observed that changes in the vibrating parameters caused resonant phenomena in a vibrofluidized granular system after a series of operations. The process by which we obtained a vibrating resonance is described below.

We set a frequency f_0 of the vertical vibration and increased the vibrating intensity. As previously reported, a pattern (e.g., a subharmonic wave) [19–21] could potentially arise on the surface of the system. The frequency of the subharmonic wave was half of the vibrating frequency, i.e., $f_0/2$. We terminated the increase in the vibrating intensity and rapidly decreased the vibrating frequency to $f_0/2$. Soon afterwards, no changes were noticed in the subharmonic wave, and a vibrating frequency temporarily equal to the frequency of the subharmonic wave was obtained. The energy absorbed by the granular system in each vibration cycle reached its maximum; that is, a vibrating resonance with a frequency $f_0/2$ occurred in the system. The vertical displacement of the resonant granules was much higher than that of the old subharmonic wave. The vibrating resonance continued for several seconds until the old $f_0/2$ subharmonic wave disappeared completely. Then a new pattern with a frequency $f_0/4$ appeared on the surface of the system. The operations producing the vibrating resonance continued, and the next resonant frequency was $f_0/4$. Apparently, the vibrating resonance depended on the sudden decrease in the vibrating frequency to half of its initial value.
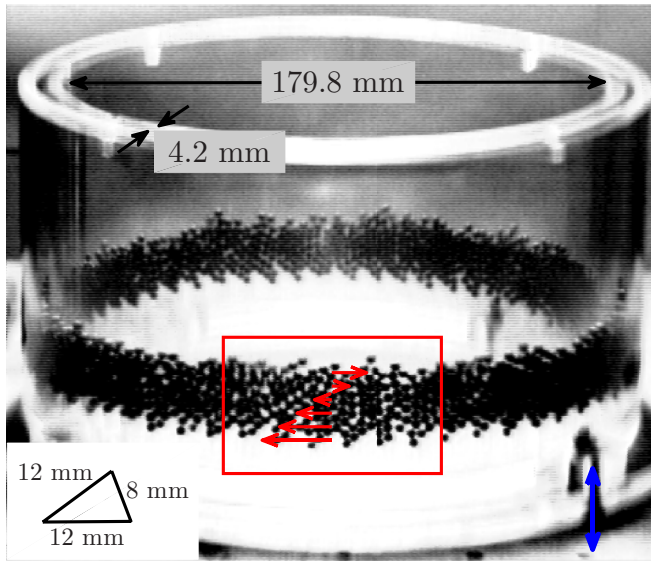
*caihui@ycit.edu.cn

FIG. 1. Panoramic view of an annular granular system. The dimensions of the container and a sawtooth are marked. The red rectangle represents a local region in which the horizontal granular flow is studied. The region has a horizontal length of seven sawteeth and includes the entire vertical height of the granular system. The superimposed red arrows in the region denote the spatial flowing distribution schematically. The blue arrow indicates the vertical vibration of the container.
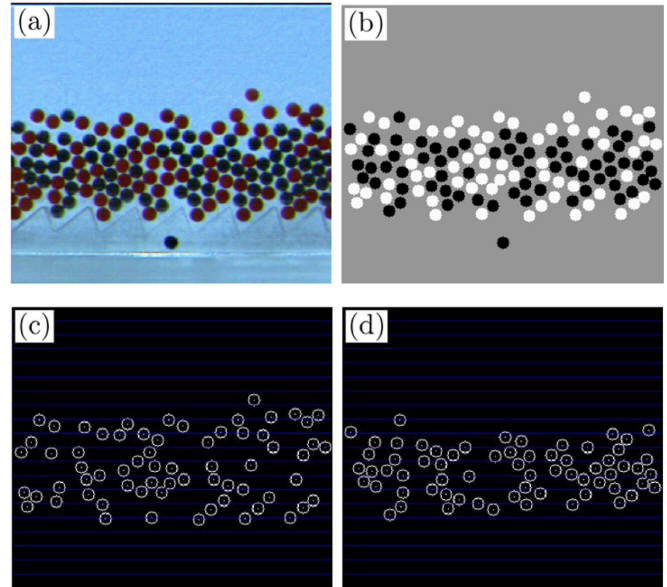

FIG. 2. Image processing. (a) Original image of a local region. The red circles represent glass spheres, and the black circles (except the lowest one) represent aluminum spheres. The lowest black circle is a marker to identify the harmonic motion of the container. (b) Gray image of the original one. All complete circles are denoted by values of 1 (white) and 0 (black) of the image matrix. (c) Centers and edges of the glass spheres in the gray image. The image is divided into N_h layers. (d) Centers and edges of the aluminum spheres.

In addition to the vibrating resonance that occurred in the subharmonic wave described above, the vertical vibration could induce other resonant phenomena in many processes happened in a granular system, for instance, the processes of transportation [22–25] and segregation [26–28]. Furthermore, the resonances in the granular system could occur at different values of parameters, such as vibrating frequency, vibrating intensity, and the mixing ratio of a binary granular system.

Here, we focused on the resonance that occurred in the granular flow in binary granular mixtures and pure granular systems; that is, the flowing resonance. The process of the flowing resonance at different parameters was described. Using a collisional model of rigid objects, we performed a preliminary theoretical exploration of the flowing resonance. These findings provide insights into the properties of granular materials under external excitation.

II. EXPERIMENTAL SETUP AND METHOD

We used two-dimensional annular granular systems [29,30] to study the flowing resonance. The systems were placed on an asymmetric periodic base (Fig. 1). Through the ratchet on the base [31–35], continuous horizontal granular flows were then generated in the systems under vertical vibration [36–38].

We employed two types of granules, opaque aluminum spheres and transparent glass spheres; these two types of spheres had different hardness and were separated during the image processing (Fig. 2). All granules had an identical diameter of 4.0 ± 0.03 mm. The total number of the granules was 1000, and the number of each type of granules was

variable. Two concentric upright plexiglass cylinders formed the annular container. The mean diameter of the cylinders was 179.8 mm, and the gap between the cylinders was 4.2 mm. Consequently, a two-dimensional granular system was effectively produced. The base of the container had a sawtooth-shaped profile. Each of the sawteeth was triangular with a length of 12 mm of the left side, 8 mm of the right side, and 12 mm of the base. The thickness of the granular system was approximately seven times of the granule diameter value. The container was mounted on a vertically vibrating exciter (Brüel & Kjær Type 4805), which vibrated sinusoidally over time. The vibrating frequency f varying from 14–24 Hz, the dimensionless vibrating acceleration $\Gamma = 4\pi^2 f^2 A/g$ (A is the vibrating amplitude, and g the gravitational acceleration) varying from 3.2–6.8, and the ratio of aluminum granules to glass granules varying from 0–1, were used as three control parameters. We commenced the experiment by uniformly stirring the granules. The granular system was then vertically vibrated at fixed values of f and Γ. The vibration lasted for several minutes until a steady horizontal granular flow was formed in the system.

A high-speed digital camera (Redlake Imaging Motion-Scope PCI 2000 SC Image Acquisition System) was utilized to record the motion of the granules for the investigation of the granular flow. Since the camera could not visualize the whole circumference of the container and therefore failed to record the motion of all granules simultaneously, we chose a local representative region along the circumference of the container for data analysis [Fig. 2(a)]. The mean horizontal granular flow was continuous in the annular container; the continuity

guaranteed that the data from any local region would yield the same results of the granular flow as those obtained from any other local region. To verify the continuity of the horizontal flow, we recorded the motion of the granules in several different positions along the circumference of the container and obtained the same results for the horizontal granular flow. A phase-locked loop frequency multiplier was employed to generate external trigger signals to control the high-speed digital camera to record at a rate of 20 frames per vibrating period T; i.e., the sample interval was $\delta t = T/20$. The size of the image recorded was 320×280 pixels, and each pixel had a spatial resolution of approximately 0.23 mm^2. A high-speed image-processing technique [39–42] was used to track the motion of the granules within the laboratory reference frame [Figs. 2(b)–2(d)]. For each group of control parameters, 4000 frame images were recorded every time; the recording was repeated at least three times.

Each of the images of the local region was divided vertically into a number of layers, each with a height δh and indicated by $1, 2, 3, \dots, N_h$ from bottom to top [Figs. 2(c) and 2(d)]. Calculate the average horizontal velocity of the aluminum granules $v_h^{(1)}(f, \Gamma, j, k)$ and glass granules $v_h^{(2)}(f, \Gamma, j, k)$, and the average number density of the aluminum granules $\rho^{(1)}(f, \Gamma, j, k)$ and glass granules $\rho^{(2)}(f, \Gamma, j, k)$, where $j = 1, 2, 3, \dots, N_h$ represents the jth layer, $k = 0, 1, 2, 3, \dots$ represents $0, \delta t, 2\delta t, 3\delta t, \dots$ instants, respectively. The horizontal granular flow at the jth layer is the sum of the aluminum horizontal flow $F_s^{(1)}(f, \Gamma, j)$ and the glass horizontal flow $F_s^{(2)}(f, \Gamma, j)$, and is given by

$$
\begin{aligned}
&F_s^{(1)}(f, \Gamma, j) + F_s^{(2)}(f, \Gamma, j) \\
&= \frac{1}{2T} \sum_{k=1}^{2T/\delta t} \big[\rho^{(1)}(f, \Gamma, j, k) v_h^{(1)}(f, \Gamma, j, k) \\
&\quad + \rho^{(2)}(f, \Gamma, j, k) v_h^{(2)}(f, \Gamma, j, k) \big] \delta h \delta t.
\end{aligned}
\tag{1}
$$

The total horizontal granular flow is the sum of the total aluminum horizontal flow $F_h^{(1)}(f, \Gamma)$ and the total glass horizontal flow $F_h^{(2)}(f, \Gamma)$, given by

$$
F_h^{(1)}(f, \Gamma) + F_h^{(2)}(f, \Gamma) = \sum_{j=1}^{N_h} \big[F_s^{(1)}(f, \Gamma, j) + F_s^{(2)}(f, \Gamma, j) \big].
\tag{2}
$$

In the following paragraphs, the behavior of the horizontal granular flow was analyzed in terms of the height distribution of horizontal flow for different vibrating accelerations and the dependence of total horizontal flow on vibrating acceleration for different vibrating frequencies and different mixing ratios of the two types of granules. From the results obtained, we confirmed the occurrence of resonances in the horizontal granular flow.

velocity fields, we can describe the motion of granular layers in a vibrating period.

At instant t_1, the granular mixture collided with the sawtooth-shaped base [Fig. 3(a)]. During the collision, the bottom layer of the mixture with rightward horizontal velocity initially collided with the left long sides of the sawteeth, and then was reflected leftwards by the long sides. At this point, the effect of the long sides dominated any effect of the short sides on the bottom layer. Defining the leftward direction as positive, we observed significantly increased horizontal velocity of the bottom layer. That was due to the increase in the positive horizontal momentum obtained by the granules in the bottom layer from the impact with the base. Almost simultaneously, at instant t_2, the bottom layer collided with the layer above it [Fig. 3(b)]. Further, the layer-layer collision transferred the positive horizontal momentum upwards from the bottom layer. The vertical velocities of the granules decreased rapidly where the layer-layer collision took place. At this instant, the collisional area was thin, but the layer-layer collision continued and moved upwards. At instant t_3, the collisional area had already become exceedingly thick [Fig. 3(c)]. This was because the greatest horizontal momentum was transferred and thereby resulted in the involvement of more granules in the transfer of the horizontal momentum. Then, at instant t_4, the layer-layer collision moved to the middle layer, and the collisional area thinned down gradually again [Fig. 3(d)]. Eventually, when the mixture separated from the base, the collision between the granular mixture and the base lasted until instant t_5 [Fig. 3(e)]. After that separation, the layer-layer collision inside the mixture continued for some time. During this period, the horizontal velocities of the lower layers decreased and even reversed. This is because that the granular mixture no longer obtained positive horizontal momentum from the base, and the continuing layer-layer collision transferred the horizontal momentum from the bottom upwards. The collisional area became extremely thin. The layer-layer collision gradually weakened as the momentum was transferred and finally ceased [Fig. 3(f)]. The horizontal velocity distribution of the mixture remained almost unchanged. The granular mixture fell down freely under gravity until it collided with the base again.

The above description shows that the transfer of the horizontal momentum was nonuniform. In the lower layers, the horizontal momentum was transferred fast and to a great extent, whereas in the upper layers, it was transferred slowly and to a low degree. We called the layer-base collision and the series of layer-layer collisions from bottom to top a complete chain-type inelastic collision. The chain-type collision may take place more than once in a vibrating period; that is, the bottom layer may collide with the base for the second time immediately after the first layer-layer collision, obtaining a horizontal momentum from the base and transferring it upwards once again.

III. RESULTS AND DISCUSSION

In our experiments, the granular mixture exhibited no significant segregation. The two types of granules were generally uniformly distributed. Figure 3 displays the velocity fields of a granular mixture at several contiguous instants. From these

A. Flow vs height

We calculated the average horizontal flow in each layer based on the velocity fields and the number density distributions of granules (results are not shown here). Then, we analyzed the distribution of the horizontal granular flow with
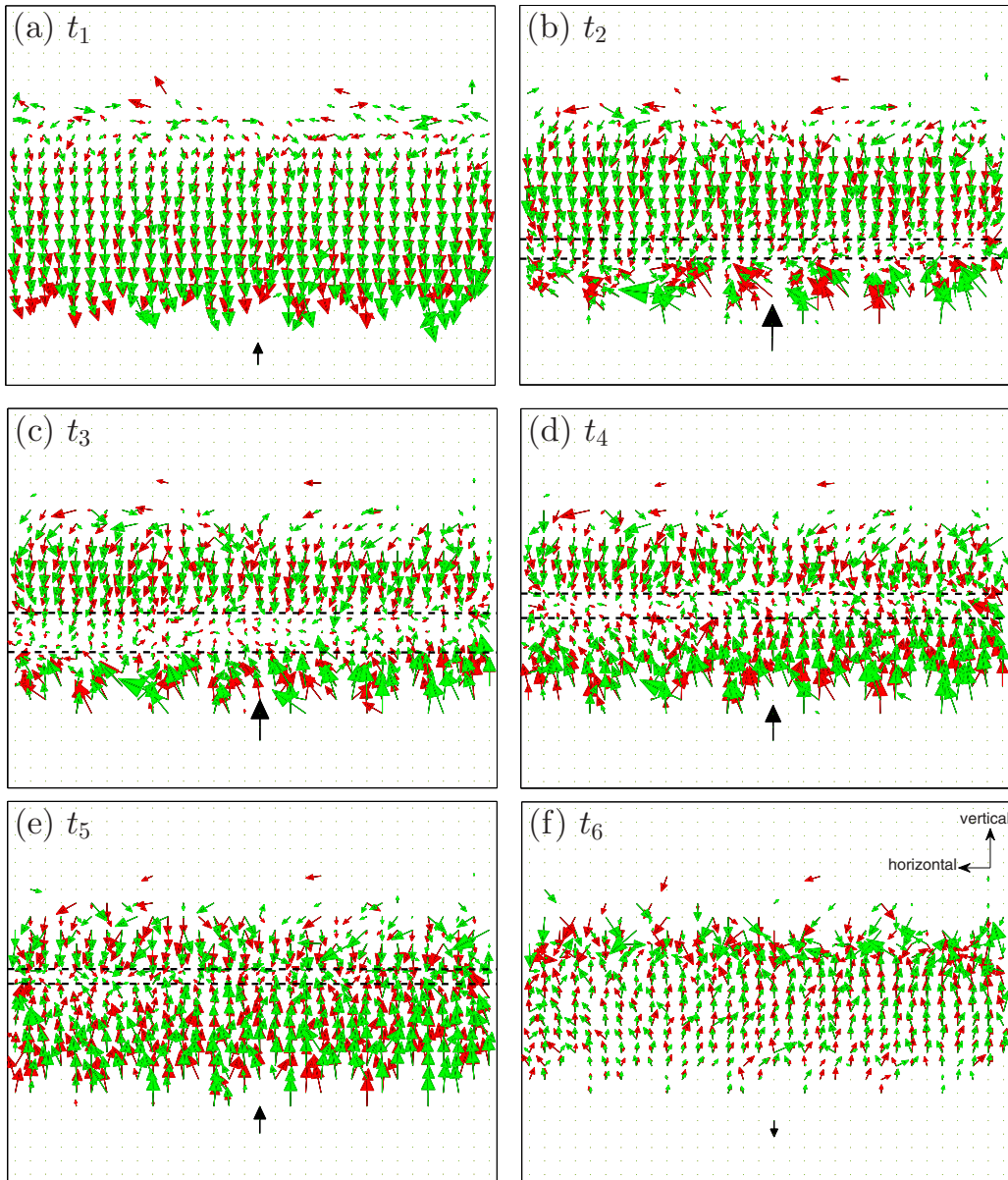
FIG. 3. Velocity fields of the granular mixture with 50% aluminum spheres and 50% glass spheres for $f = 16$ Hz and $\Gamma = 5.0$. The red arrows represent the velocities of the aluminum spheres, and the green arrows represent the velocities of the glass spheres. The lowest black arrow represents the velocity of the base. The dashed lines in (b)–(e) outline the collisional areas at these instants. The positive horizontal and vertical directions are shown in the top right of Fig. 3(f).

the changes in height [Eq. (1) and Fig. 4(a)]. The thickness of layers occupied by the horizontal flow increased with the rise in vibrating acceleration Γ. This was because the increased Γ promoted the fluidization of the granular system, leading to the spread of granules into more layers. In general, the granular mixture had a positive horizontal flow or a negative horizontal flow in each layer. The bottom layers were characterized by a positive flow, but the positive flow changed slightly along with the variation in vibrating acceleration. The increase in height reversed the horizontal flow into negative for the first time. The negative horizontal flow was particularly prominent when $\Gamma = 4.8$. The thickness of layers, which had a negative horizontal flow first increased then decreased with the rise in Γ. As the height was continuously elevated, the horizontal flow reversed to a positive flow again. The

amplitude of the positive flow and the thickness of layers with the positive flow significantly increased after $\Gamma = 4.8$. However, in the higher layers, the horizontal flow decreased and became negative for the second time, and finally changed into positive in the top layers. The horizontal flow in the top layers was exceedingly low since the layer-layer collision was weak on the top, and the horizontal momentum transferred was rather small.

The height distributions of the aluminum flow and glass flow in the granular mixture were similar to that of the mixing flow [Fig. 4(b)]. For each Γ, the height distribution of the aluminum flow was higher than that of the glass flow; the glass flow was greater than the aluminum flow in most layers. These results indicated that the aluminum granules flowed more slowly and were more dispersed than the glass granules.
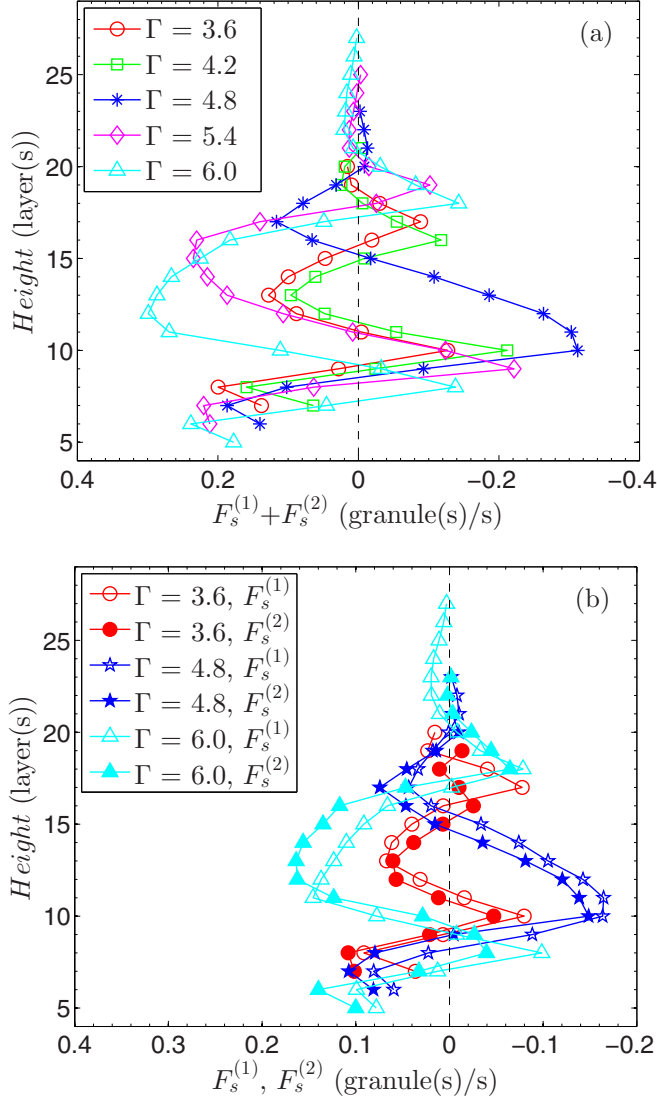
FIG. 4. Stratified horizontal flow as a function of height for (a) the granular mixture with 50% aluminum spheres and 50% glass spheres; (b) the 50% aluminum spheres and 50% glass spheres of the granular mixture. Here, $f = 20$ Hz.
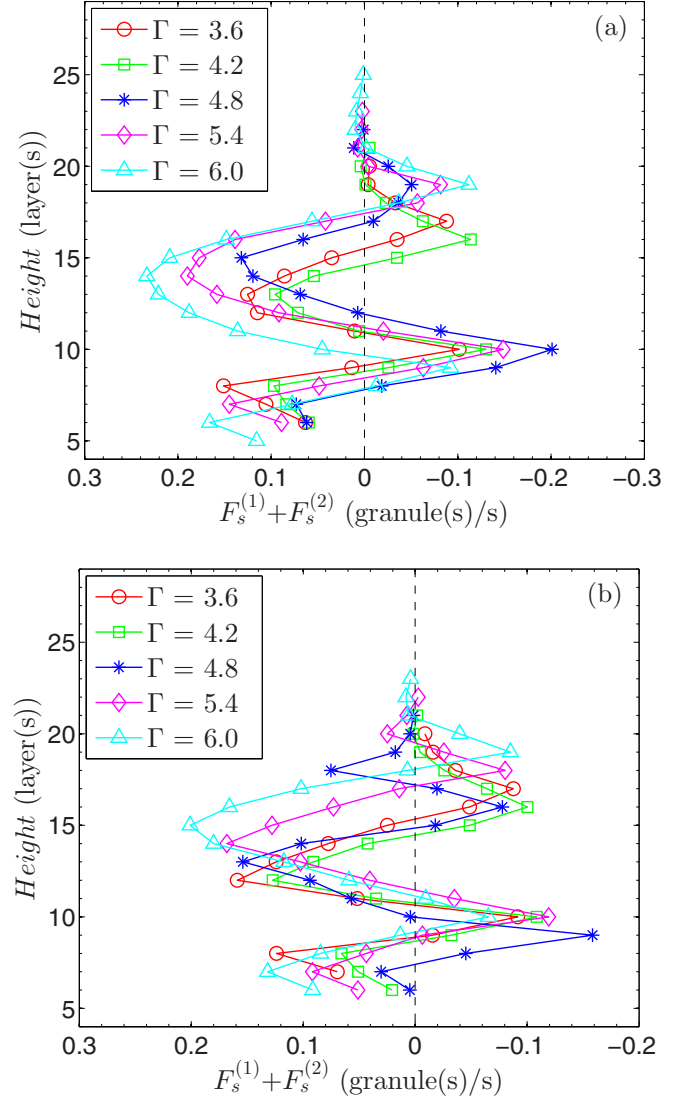

FIG. 5. Stratified horizontal flow as a function of height for (a) the granular mixture with 75% aluminum spheres and 25% glass spheres; (b) the pure aluminum granular system. Here, $f = 20$ Hz.

For other granular systems with different mixing ratios, the horizontal flow ordinarily had alternating, positive-negative-positive-negative-positive values varying from the bottom to the top layers (Fig. 5); this was similar to the fluctuations of the mixing flow with height elevation described in Fig. 4(a). However, as the number of aluminum granules increased, the thickness of layers the horizontal flow occupied decreased, and the amplitude of the stratified horizontal flow decreased as well. For the pure aluminum granular system [Fig. 5(b)], the positive horizontal flow in the bottom layer was considerably changed with different vibrating accelerations. The height of the negative horizontal flow in the lower layers reached a minimum when $\Gamma = 4.8$; the thickness of layers with the negative flow changed only slightly with Γ alterations. The height of layers with a positive horizontal flow after the second reversal increased with Γ rising; the thickness of layers with the positive flow also increased slightly with Γ elevation. Small changes were observed in the amplitude of

a negative horizontal flow with Γ rising in the higher layers; the height of layers with the negative flow first decreased then increased with Γ rising. The positive horizontal flow in the top layers diminished with the rise in Γ after $\Gamma = 4.8$, whereas the height of layers with the positive flow was augmented with Γ elevation. All these fluctuations were significantly different from that in the granular mixture described in Fig. 4(a).

B. Collisional model

The difference in the height distributions of the horizontal granular flow between different granular systems was caused by the change in the inelastic collisions; that is, the change in the coefficient of restitution. To determine the properties of the horizontal granular flow, we constructed a collisional model of rigid objects by simplifying the interactions between the granules. We considered the base and each layer as rigid objects. The layer-base collision and layer-layer collisions were oblique because of the asymmetric periodic structure
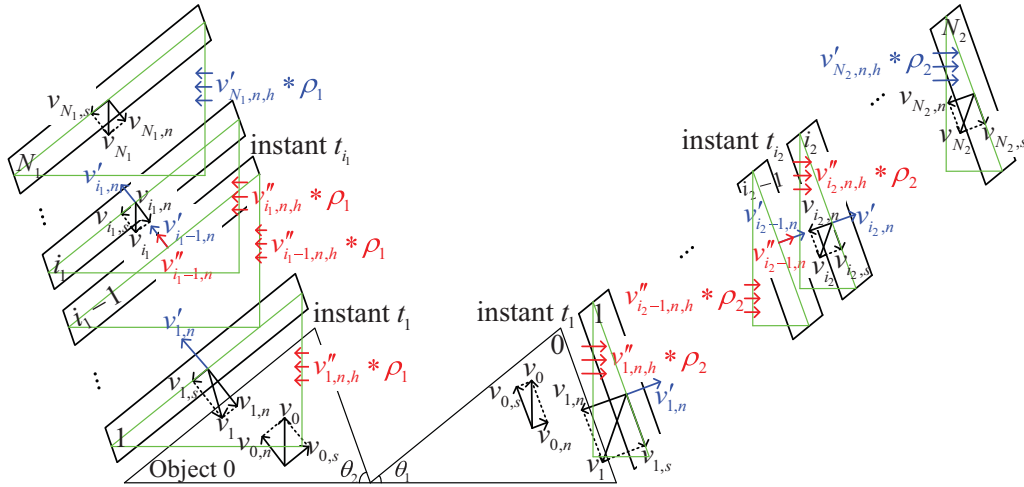
FIG. 6. Collisional model of rigid objects for layer-base and layer-layer collisions. The chain-type collision with N_1 objects is caused by the left long side of each sawtooth, and the chain-type collision with N_2 objects is caused by the right short side of each sawtooth. The first precollisional velocity of each object is decomposed into normal velocity (denoted by subscript n) and shear velocity (denoted by subscript s). The first postcollisional normal velocity (denoted by superscript $'$) is the second precollisional normal velocity. The second postcollisional normal velocity (denoted by superscript $''$) is decomposed into a horizontal velocity (denoted by subscript h) and a vertical velocity (not shown in the figure). The superimposed arrows on each green triangle represent schematically the horizontal flow caused by the rigid object after a complete chain-type collision.

of the base. Then, we presumed that each oblique chain-type inelastic collision (including a layer-base collision and a series of layer-layer collisions) could be replaced by two separate chain-type collisions between rigid objects, with one collision occurring on the left long side of a sawtooth (left chain-type collision, abbreviated and denoted as LCTC), and the other on the right short side (right chain-type collision, abbreviated and denoted as RCTC) (Fig. 6). We then decomposed each object-object inelastic collision into normal collision perpendicular

to the side of a sawtooth and shear friction parallel to the side. The shear friction caused rotation of the granules, but we neglected its effect on the motion of the rigid objects for simplicity. The normal collision gave rise to velocity variations of the rigid objects (and granules) in both the horizontal and the vertical directions.

The formula for the velocities of two adjacent objects i and $i-1$ after a normal collision is given by the equations

$$
\begin{aligned}
v'_{i,n} &= v_{i,n} + \frac{m_{i-1}}{m_{i-1} + m_i}(1 + e_{i,i-1})(v'_{i-1,n} - v_{i,n}) \\
v''_{i-1,n} &= v'_{i-1,n} - \frac{m_i}{m_{i-1} + m_i}(1 + e_{i,i-1})(v'_{i-1,n} - v_{i,n})
\end{aligned}
\quad \text{(where } i > 1\text{),}
\tag{3}
$$

where $v'_{i,n}$ and $v_{i,n}$ are the postcollisional and precollisional velocities of the object i in the normal collision between object i and object $i-1$, respectively; $v''_{i-1,n}$ and $v'_{i-1,n}$ are the postcollisional and precollisional velocities of object $i-1$ in the normal collision, respectively (Each rigid object, except for the bottom and the top objects, occurs two collisions in a complete chain-type collision. The precollisional velocity $v'_{i-1,n}$ of the normal collision between object i and object $i-1$ is the postcollisional velocity of the normal collision between object $i-1$ and object $i-2$. The object $i-1$ obtains the second postcollisional velocity $v''_{i-1,n}$ after colliding with the object i. The bottom object 0, which represents the base of the container, has a postcollisional velocity $v'_{0,n}$ and a precollisional velocity $v_{0,n}$, which satisfies $v'_{0,n} = v_{0,n}$); m_i is the mass of object i (The mass of the base m_0 is regarded as infinity. The masses of other objects are finite and equal); $e_{i,i-1}$ is the coefficient of restitution of the normal collision between object i and object $i-1$, which varies from 0 to 1 (Here $e_{i,i-1}$ is used to indicate different granular systems.

It decreases as the ratio of the aluminum granules increases. For the chain-type collision between rigid objects, it could be considered a constant. For discrete granular layers, previous findings show that $e_{i,i-1}$ decreases as the number density of granules increases, and it is dependent on the collisional velocities [43–46]). The horizontal flow at the jth layer produced by LCTC and RCTC is given by

$$
\begin{aligned}
F_s(f, \Gamma, j) &= \sum_{i_1=1}^{N_1-1} v''_{i_1,n,h}(f, \Gamma, j) * \rho_1 + v'_{N_1,n,h}(f, \Gamma, j) * \rho_1 \\
&\quad - \sum_{i_2=1}^{N_2-1} v''_{i_2,n,h}(f, \Gamma, j) * \rho_2 \\
&\quad - v'_{N_2,n,h}(f, \Gamma, j) * \rho_2,
\end{aligned}
\tag{4}
$$

where the subscript i_1 represents the i_1th object of LCTC with N_1 objects, the subscript i_2 represents the i_2th object of RCTC

with N_2 objects, the subscript h represents the horizontal component of a normal velocity, ρ_1 and ρ_2 represent the densities of the objects of LCTC and RCTC, respectively. The horizontal flow produced by each object distributes at different heights. The leftward horizontal flow generated by each object of LCTC is positive, whereas the rightward horizontal flow produced by each object of RCTC is negative. Each object-object collision is of short duration, and its strength is reduced after several complete chain-type collisions. Finally, the velocities of all objects are almost the same after all the collisions. The height distribution of the horizontal flow after three complete chain-type collisions is illustrated in Fig. 7.

Many similarities existed between the stratified horizontal flows observed in the collisional model [Eq. (4) and Fig. 7(a)] and the experiments. For instance, when Γ was fixed, the horizontal flow reached its minimum after one reversal, whereas it reached its maximum after two reversals; when Γ was variable, the horizontal flow reached its minimum at $\Gamma = 4.8$, while it reached its maximum at $\Gamma = 6.0$. The amplitude of the stratified horizontal flow was near to the one presented in our experimental results. On the other hand, there were also some differences. The horizontal flow given by the collisional model was situated at the same height for different vibrating accelerations; this was because rigid objects could not expand along with the increase in Γ. The stratified horizontal flow had positive-negative-positive-negative values from bottom to top; the flow was reversed fewer times than the experimental results. The variation of the horizontal flow with height for each Γ was nonmonotonic after the flow reached the minimum and the maximum. As the coefficient of restitution e changed, the inelastic collisions between rigid objects were altered, resulting in different height distributions of the horizontal flow [Figs. 7(b) and 7(c)]. The decrease in e led to a reduction in the amplitude of the stratified horizontal flow; this reduction was consistent with the experimental findings.

The stratified horizontal flows that were obtained in the experiments and the collisional model had similar distributions and variations. This outcome implies that it is reasonable to simplify the interactions between the granules with LCTC and RCTC. The collisional model of rigid objects improves the current understanding of the mechanism of the horizontal granular flow.

C. Flow vs vibrating parameters

We added the horizontal flows of all layers to obtain the total horizontal flow of the granular mixture. Figure 8(a) illustrates the variation of the total horizontal flow with the vibrating acceleration for different vibrating frequencies [Eq. (2)]. For each vibrating frequency f, the total horizontal flow varied continuously along with the vibrating acceleration Γ and had two rising stages. These two stages of elevation corresponded to the subharmonic waves with frequencies $f/2$ and $f/4$, respectively, when the granular system was completely fluidized. In the two rising stages, a higher value of Γ led to a more elevated vertical position of the granular system, which in turn resulted in a more horizontal momentum the system received from the collision with the base, further promoting the horizontal flow. The falling stages in each variation of the total horizontal flow with Γ were caused by
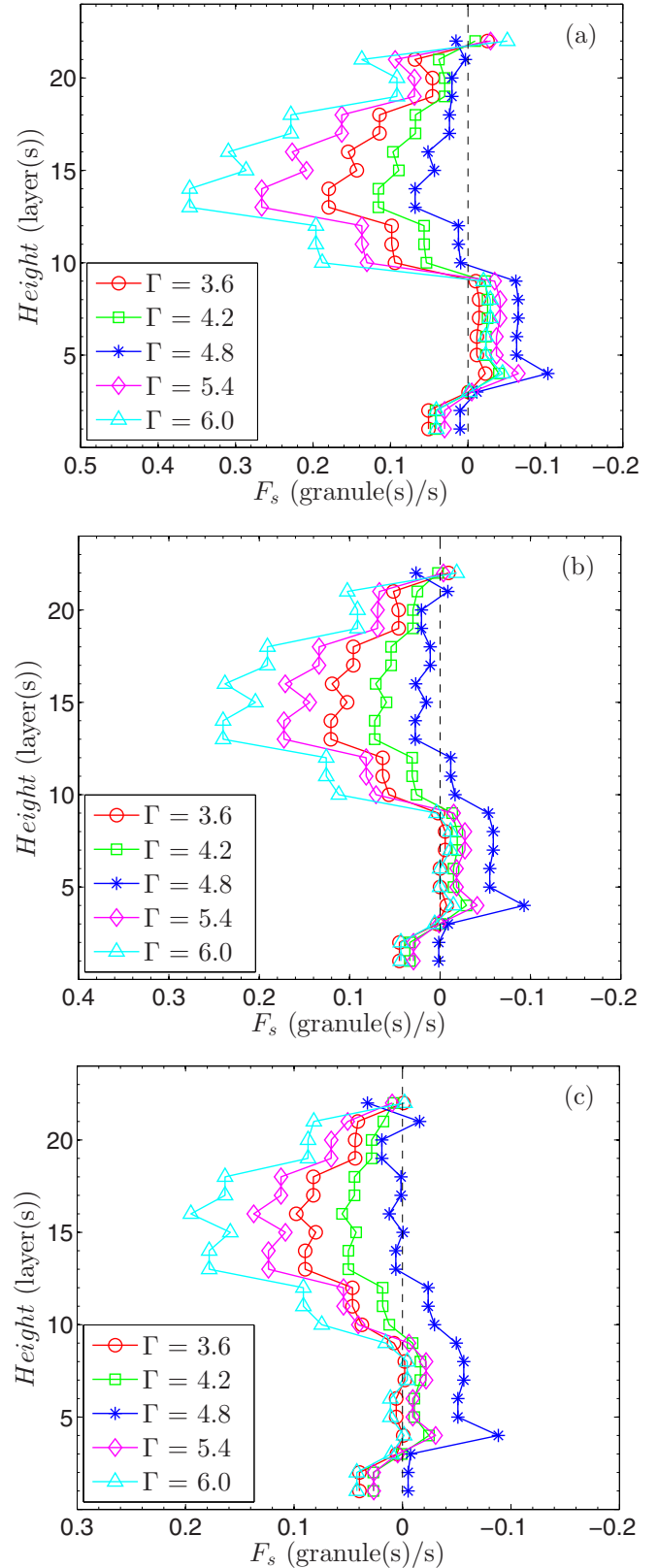

FIG. 7. Stratified horizontal flow as a function of height for the rigid objects after three complete chain-type collisions at $f = 20$ Hz and five vibrating accelerations. The values of N_1 and N_2 are 6 and 9, respectively. The coefficients of restitution are (a) $e = 0.6$, (b) $e = 0.5$, and (c) $e = 0.4$. Here, e decreasing means the ratio of the aluminum granules increasing.
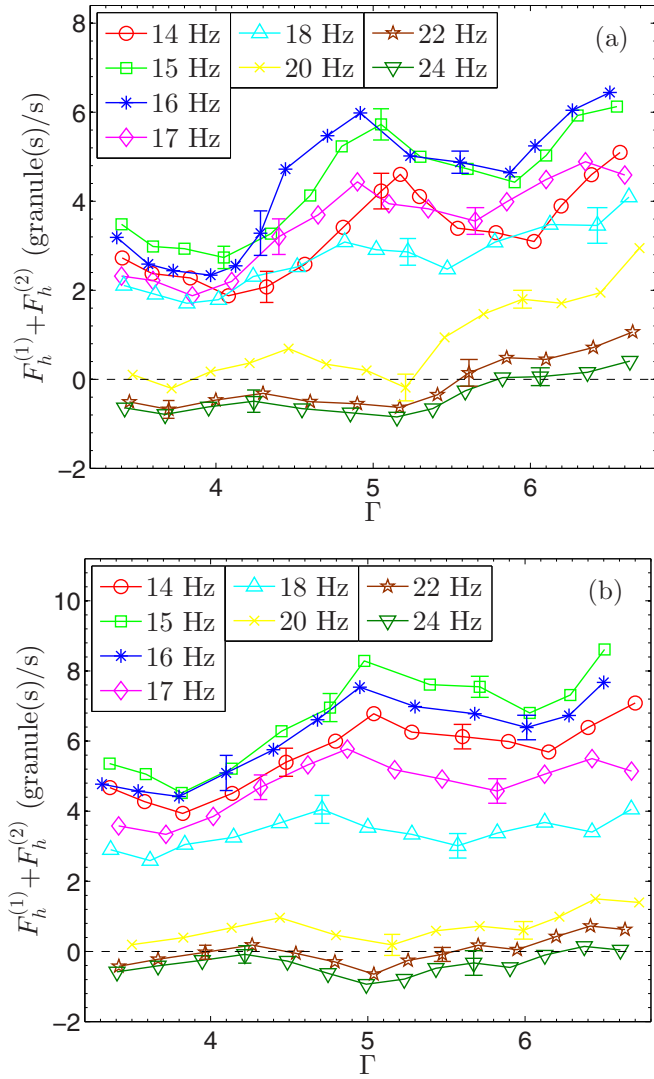
FIG. 8. Total horizontal flow as a function of vibrating acceleration at different vibrating frequencies for the granular mixtures with (a) 50% aluminum spheres and 50% glass spheres; (b) 25% aluminum spheres and 75% glass spheres. Error bars are depicted on each curve.

the combined motion of the granules at weak fluidization of the system. The combined motion of the granules caused a negative horizontal flow at some Γ's, when $f \geqslant 20$ Hz. In this mixture, the horizontal flow at $f = 15$ Hz competed with the flow at $f = 16$ Hz.

As the ratio of the glass granules increased, the total horizontal flow increased in general, indicating that the glass granules in the mixture facilitated the increase in the total horizontal flow [Fig. 8(b)]. The variation of the total horizontal flow with the vibrating parameters became moderate. It is worth noting that at a frequency of 15 Hz, the horizontal flow reached the maximum for each of the vibrating accelerations. The total horizontal flows at $f = 14$ Hz and $f \geqslant 16$ Hz were both smaller than that at $f = 15$ Hz. The horizontal flow at $f = 24$ Hz was the lowest and almost completely negative, as can be seen in Fig. 8(b). This variation of the total horizontal flow with f was caused by two opposite effects of f on the

flow. On the one hand, at a constant Γ, a higher f value resulted in more frequent collisions of the granular system with the base, increasing the horizontal momentum of the granules obtained from the base per unit time and promoting a greater horizontal flow. On the other hand, at the higher f value, the vibrating amplitude at the fixed Γ was insignificant; the horizontal momentum of the granules received from the base was lower, and the horizontal flow was minor. These two opposite actions augmented the horizontal flow to its maximum at $f = 15$ Hz.

We believed that a resonance occurred in the total horizontal flow for the vibrating frequency of 15 Hz. After the decomposition of the oblique collisions between the granular system and the base, the horizontal motion of the granular system in a vibrating period could be explained as follows. The granular system initially moved in the negative horizontal direction, followed by a collision with the base. Next, the base pushed the granular system to the positive horizontal direction. However, the positive horizontal velocity of the granular system decreased with time, and its direction was finally reversed. When the horizontal velocity of the granular system decreased to its precollisional value, the base pushed the granular system for the second time. The granular system obtained a net horizontal displacement during the back-and-forth movement. Generally, the periodic movement of the granular system has a natural frequency. When the pushing frequency of the base matches the natural frequency of the granular system, the horizontal displacement of the granular system reaches its maximum; that is, a flowing resonance occurs. For each granular system, there is a vibrating frequency that leads the horizontal flow to a maximum. Here, the granular system acted as a pendulum in the horizontal direction. Relevant research concerning the natural frequency of a vibrofluidized granular system has not been reported. It is worthy of intensive exploration.

As can be observed in Fig. 9, the total horizontal flow in the pure aluminum system is rather different from that in the
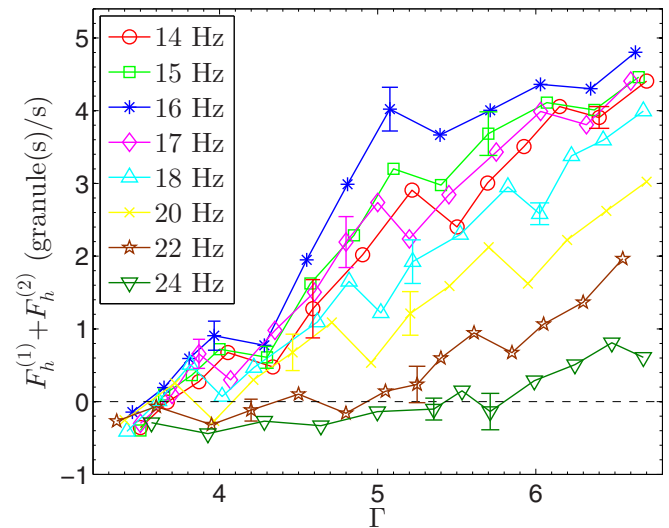

FIG. 9. Total horizontal flow as a function of vibrating acceleration at different vibrating frequencies for the pure aluminum granular system. Error bars are depicted on each curve.
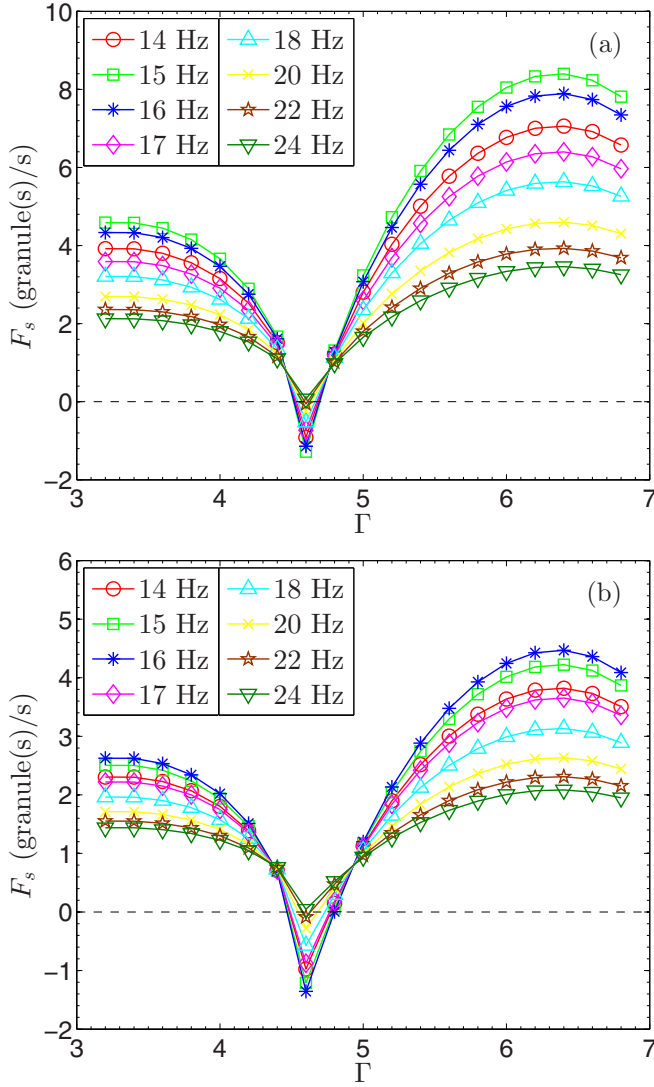
FIG. 10. Total horizontal flow of the rigid objects as a function of vibrating acceleration at different vibrating frequencies for (a) $e = 0.7$ and (b) $e = 0.4$. Here, three complete chain-type collisions have occurred.

granular mixtures described in Fig. 8. At a lower Γ value, the change in f caused no significant difference in the total horizontal flow. However, the difference increased with the augmentation of Γ value. The total flow at $f = 16$ Hz was gradually but considerably enhanced with the elevation in Γ, while the total flow at $f = 24$ Hz varied moderately. At $f < 22$ Hz, the total horizontal flow was always positive for $\Gamma > 4.0$, while at $f > 22$ Hz, the total horizontal flow was negative for most of the vibrating accelerations. The variation of the total horizontal flow with Γ for each vibrating frequency usually consisted of two or more rising stages. The flowing resonance occurred in the pure granular system as well, and the resonant flow for $f = 16$ Hz increased substantially with the elevation in Γ.

Figure 10 represents the variation in the total horizontal flow with vibrating parameters given by the inelastic collisional model of rigid objects. The total horizontal flow experienced two rising and two falling stages within the range

of Γ values studied. The second rising stage increased the flow to the maximum, and the first falling stage diminished the flow to the minimum. When the coefficient of restitution e took a higher value, the total horizontal flow at $f = 15$ Hz was greater than the flows at other frequencies for all vibrating accelerations, except for $\Gamma = 4.6$ at the minimum flow [Fig. 10(a)]. Interestingly, flowing resonance occurred at a frequency of 15 Hz. When e took a lower value, the flowing resonance occurred at $f = 16$ Hz [Fig. 10(b)]. These results agreed qualitatively with the experimental ones. The major differences in the total horizontal flow given by the collisional model with the flow in the experiments were that the minimum flows for different frequencies occurred at the same Γ value, and the negative flow at resonant frequency and $\Gamma = 4.6$ was the smallest. This outcome was because the falling N_1 (and N_2) rigid objects collided with the falling rigid object 0 at $\Gamma = 4.6$. The N_1 (and N_2) objects had not obtained sufficient positive momentum from object 0 to change the amplitude and direction of the total horizontal flow after three chain-type collisions. In addition, in the collisional model, the coefficient of restitution e for the chain-type collisions was regarded as a constant. Actually, previous studies conducted in the experimental systems showed that e changed with the number density of the granules and the collisional velocities between the granules [43–46].

D. Flow vs mixing ratio

The change in the mixing ratio of a granular mixture is also associated with the occurrence of flowing resonance. As depicted in Fig. 11(a), at lower f, the total horizontal flow in the pure glass system was greater than that in the pure aluminum system for all vibrating accelerations. However, when 75% glass granules were mixed with 25% aluminum granules, the total horizontal flow in this mixture was greatest. Here, the natural frequency of this granular mixture was closest to the vibrating frequency of 17 Hz; thus, a flowing resonance has occurred. For the pure aluminum granular system, the total horizontal flow increased significantly after four rising stages. The variation in the total horizontal flow with Γ was gradually moderated with the increase in the ratio of the glass granules in the mixture. After the number of glass granules exceeded half of the number of total granules, the horizontal flow changed slightly with Γ fluctuating, with the exception of reaching a maximum at an approximate value of $\Gamma = 4.8$.

Figure 11(a) also shows that, at lower Γ, the effect of the mixing ratio on the total horizontal flow was greater. This effect decreased with the rise in Γ, which could be explained as follows. As Γ increases, the fluidization of the granular system strengthens, resulting in a looser system and a week interaction between the granules. Thus, the granular systems with different mixing ratios gradually start to act identically in terms of the total horizontal flow.

The variation of the total horizontal flow with the mixing ratio at higher f seems a little chaotic [Fig. 11(b)]. There was no fixed mixing ratio resulting in the flowing resonance. At $\Gamma < 5.0$, the pure glass granular system easily produced the maximum horizontal flow; while at $\Gamma > 5.0$, the resonant system was replaced by the pure aluminum granular system.
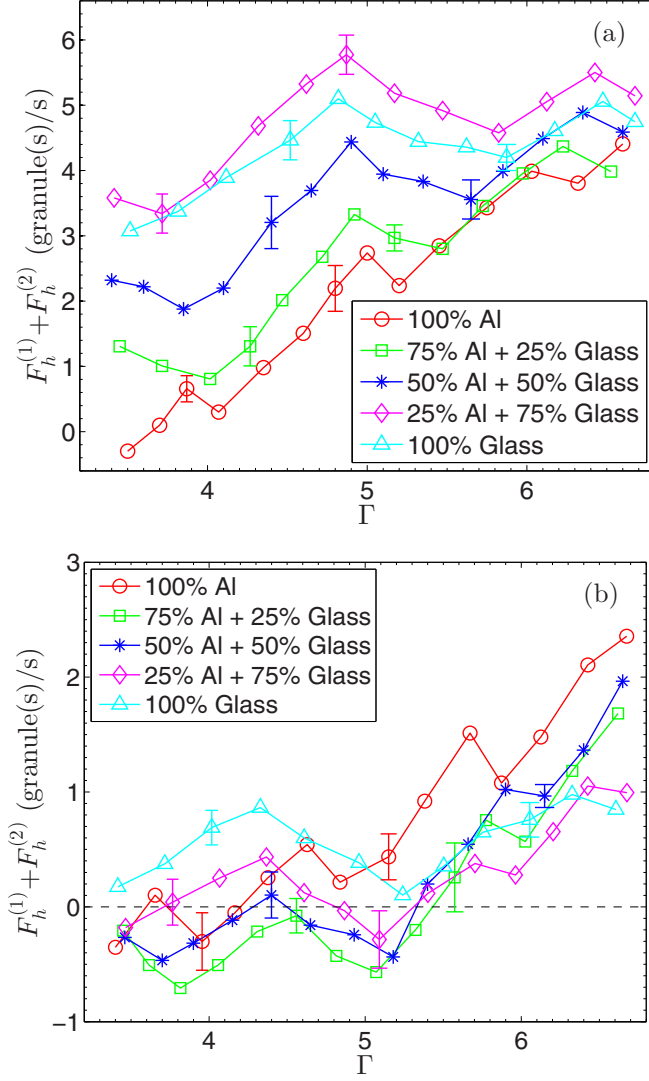
FIG. 11. Total horizontal flow as a function of vibrating acceleration for different mixing ratios of the aluminum granules and glass granules. Here, the vibrating frequencies are (a) 17 Hz and (b) 21 Hz. Error bars are depicted on each curve.

This result means that the natural frequency of a vibrated granular system could be increased by means of lowering the ratio of glass granules or the vibrating acceleration.

The coefficient of restitution in the collisional model of rigid objects varies in different granular systems. In our study, for the same vibrating parameters, e increased with the ratio of the glass granules and reached a maximum for the pure glass granular system. The collisional model presented the flowing resonance for the coefficient of restitution (Fig. 12). For each Γ except for the value 4.6, the total horizontal flow increased with e first, then reached a maximum when $e = 0.7$. After that, the flow decreased as e increased. The flow at $\Gamma = 4.6$ had little change for e, indicating that the chain-type collisions in a vibrating period occurred far more than three times under this condition.

The flowing resonances presented by both the experiments and the collisional model reveal a dynamic property of the granular materials under external vibration. More specifically,
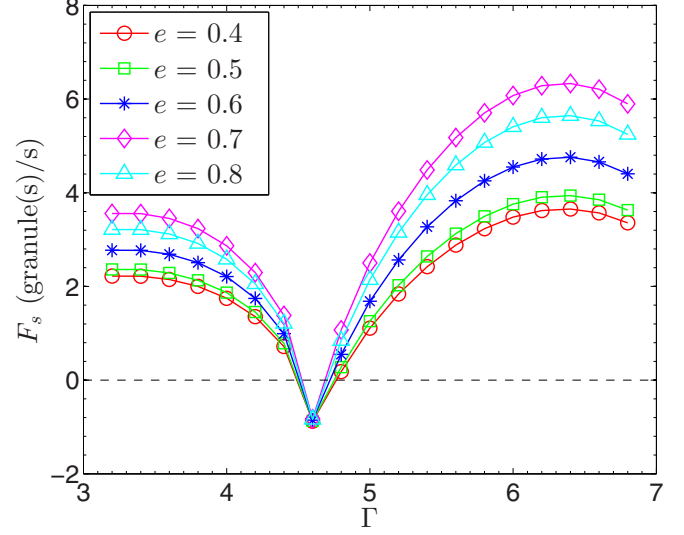

FIG. 12. Total horizontal flow of the rigid objects as a function of vibrating acceleration for different coefficients of restitution and $f = 17$ Hz. Here, three complete chain-type collisions have been finished.

the motion of the granules has a maximum response to the external vibration; the maximum response could be maximum displacement or maximum velocity. Parameters of the external vibration, such as vibrating frequency, vibrating acceleration, and vibrating amplitude, could be changed to reach the maximum response. On the other hand, to achieve that effect, we could change the properties of the granular system, such as its mixing ratio, the number of the total granules, and the material of the granules. Essentially, the resonance in a granular system is produced by the consistency between the natural frequency of the granular system and the frequency of the external vibration. Finding the natural frequency of the vibrated granular system is our undergoing research work.

IV. CONCLUSIONS

In conclusion, we observed resonant phenomena in the horizontal flow of different annular granular systems under vertical vibration. The flowing resonance occurred at a certain vibrating frequency of the base for a given mixing ratio of the binary granular system. By decomposing the motion of the granular system, we concluded that the system oscillated horizontally with a natural frequency under a periodic external force, which was exerted by the vertically vibrated asymmetric sawteeth. The natural frequency of the horizontal oscillation was dependent on the mixing ratio of the two types of granules. At a fixed mixing ratio, if the vibrating frequency was changed to match the natural frequency, one flowing resonance occurred. When a vibrating frequency was fixed, if the mixing ratio was altered to induce a natural frequency, which was close to the vibrating frequency, another flowing resonance occurred. We constructed an inelastic collisional model of rigid objects to explore their flowing resonances. The collisional model presented resonances as well, indicating that the phenomena are typical in the granular systems. However, the results obtained in the collisional model were short of differences in some details for different control parameters.

This was because the granular system was more complex than the collisional model of rigid objects. Therefore, the coefficient of restitution in a vibrated granular system constantly changes. Moreover, the number density of the granular system is a function of the vibration parameters, and the shear friction generated by the oblique collisions between the granules affects the horizontal granular flow. These factors should be considered in the development of a theoretical model.

[1] K. Ogata, *System Dynamics* (Prentice Hall, New Jersey, 2004).

[2] A. Ghatak, *Optics* (McGraw-Hill, New Delhi, 2009).

[3] R. A. Nelson and M. G. Olsson, The pendulum - Rich physics from a simple system, Am. J. Phys. **54**, 112 (1986).

[4] Y. Xu, T. J. Alexander, H. Sidhu, and P. G. Kevrekidis, Instability dynamics and breather formation in a horizontally shaken pendulum chain, Phys. Rev. E **90**, 042921 (2014).

[5] V. Y. Kuperman, Nuclear Magnetic Resonance Measurements of Diffusion in Granular Media, Phys. Rev. Lett. **77**, 1178 (1996).

[6] J. Mitchell, A. Souza, E. Fordham, and A. Boyd, A finite element approach to forward modeling of nuclear magnetic resonance measurements in coupled pore systems, J. Chem. Phys. **150**, 154708 (2019).

[7] H. Nadeem and T. J. Heindel, Review of noninvasive methods to characterize granular mixing, Powder Technol. **332**, 331 (2018).

[8] F. Melo, P. Umbanhowar, and H. L. Swinney, Transition to Parametric Wave Patterns in a Vertically Oscillated Granular Layer, Phys. Rev. Lett. **72**, 172 (1994).

[9] F. Melo, P. B. Umbanhowar, and H. L. Swinney, Hexagons, Kinks, and Disorder in Oscillated Granular Layers, Phys. Rev. Lett. **75**, 3838 (1995).

[10] P. Maynar, M. I. García de Soria, and J. J. Brey, Understanding an instability in vibrated granular monolayers, Phys. Rev. E **99**, 032903 (2019).

[11] I. H. Ansari, N. Rivas, and M. Alam, Phase-coexisting patterns, horizontal segregation, and controlled convection in vertically vibrated binary granular mixtures, Phys. Rev. E **97**, 012911 (2018).

[12] D. Tsuji, M. Otsuki, and H. Katsuragi, Relaxation Dynamics of a Granular Pile on a Vertically Vibrating Plate, Phys. Rev. Lett. **120**, 128001 (2018).

[13] A. Mehta and J. M. Luck, Novel Temporal Behavior of a Nonlinear Dynamical System: The Completely Inelastic Bouncing Ball, Phys. Rev. Lett. **65**, 393 (1990).

[14] M. Hubert, F. Ludewig, S. Dorbolo, and N. Vandewalle, Bouncing dynamics of a spring, Phys. D: Nonlinear Phenomena **272**, 1 (2014).

[15] Z. H. Jiang, Y. Y. Wang, and J. Wu, Subharmonic motion of granular particles under vertical vibrations, Euro. Phys. Lett. **74**, 417 (2006).

[16] J. A. F. Balista and C. Saloma, Modified inelastic bouncing ball model of the Brazil nut effect and its reverse, Granul. Matter **20**, 47 (2018).

[17] N. Loguinova, Resonance in a granular system, Granul. Matter **11**, 63 (2009).

[18] C. R. K. Windows-Yule, A. D. Rosato, A. R. Thornton, and D. J. Parker, Resonance effects on the dynamics of dense granular beds: Achieving optimal energy transfer in vibrated granular systems, New J. Phys. **17**, 023015 (2015).

[19] K. Huang, Internal and surface waves in vibrofluidized granular materials: Role of cohesion, Phys. Rev. E **97**, 052905 (2018).

[20] L. de Martín, Influence of particle dynamics on the instability for pattern formation in shallow pulsed beds, Phys. Rev. Fluids **3**, 124304 (2018).

[21] H. Cai, W. Z. Chen, and G. Q. Miao, Patterns in a two-dimensional annular granular layer, Chin. Phys. Lett. **30**, 044501 (2013).

[22] I. Derényi, P. Tegzes, and T. Vicsek, Collective transport in locally asymmetric periodic structures, Chaos **8**, 657 (1998).

[23] Z. Farkas, P. Tegzes, A. Vukics, and T. Vicsek, Transitions in the horizontal transport of vertically vibrated granular layers, Phys. Rev. E **60**, 7022 (1999).

[24] M. Levanon and D. C. Rapaport, Stratified horizontal flow in vertically vibrated granular layers, Phys. Rev. E **64**, 011304 (2001).

[25] S. Mobarakabadi, E. N. Oskoee, M. Schröter, and M. Habibi, Granular transport in a horizontally vibrated sawtooth channel, Phys. Rev. E **88**, 042201 (2013).

[26] L. Li, P. Wu, S. P. Zhang, and L. Wang, Vertical separation criterion of binary particles under external excitation, Powder Technol. **342**, 404 (2019).

[27] A. Bhateja, I. Sharma, and J. K. Singh, Segregation physics of a macroscale granular ratchet, Phys. Rev. Fluids **2**, 052301(R) (2017).

[28] J. Sun, C. P. Liu, P. Wu, Z. A. Xie, K. W. Hu, and L. Wang, Granular core phenomenon induced by convection in a vertically vibrated cylindrical container, Phys. Rev. E **94**, 032906 (2016).

[29] H. K. Pak and R. P. Behringer, Surface Waves in Vertically Vibrated Granular Materials, Phys. Rev. Lett. **71**, 1832 (1993).

[30] H. K. Pak, E. Van Doorn, and R. P. Behringer, Effects of Ambient Gases on Granular Materials under Vertical Vibration, Phys. Rev. Lett. **74**, 4643 (1995).

[31] P. Müller, J. A. C. Gallas, and T. Pöschel, Dynamical regimes and stability of circular granular ratchets, Sci. Rep. **7**, 12723 (2017).

[32] A. Gnoli, A. Petri, F. Dalton, G. Pontuale, G. Gradenigo, A. Sarracino, and A. Puglisi, Brownian Ratchet in a Thermal Bath Driven by Coulomb Friction, Phys. Rev. Lett. **110**, 120601 (2013).

[33] R. Balzan, F. Dalton, V. Loreto, A. Petri, and G. Pontuale, Brownian motor in a granular medium, Phys. Rev. E **83**, 031310 (2011).

[34] G. Costantini, A. Puglisi, and U. M. B. Marconi, Granular ratchets, Eur. Phys. J. Spec. Top. **179**, 197 (2009).

[35] D. Volfson, A. Kudrolli, and L. S. Tsimring, Anisotropy-driven dynamics in vibrated granular rods, Phys. Rev. E **70**, 051312 (2004).

[36] G. W. Baxter and J. S. Olafsen, Experimental Evidence for Molecular Chaos in Granular Gases, Phys. Rev. Lett. **99**, 028001 (2007).

[37] H. Cai, W. Z. Chen, and G. Q. Miao, Horizontal flow and surface patterns in a vertically vibrated annular granular layer, Phys. Rev. E **91**, 032204 (2015).

[38] S. Mobarakabadi, N. Adrang, M. Habibi, and E. N. Oskoee, Segregation of a binary granular mixture in a vibrating sawtooth base container, Eur. Phys. J. E **40**, 79 (2017).

[39] S. Warr, G. T. H. Jacques, and J. M. Huntley, Tracking the translational and rotational motion of granular particles: Use of high-speed photography and image processing, Powder Technol. **81**, 41 (1994).

[40] R. D. Wildman and J. M. Huntley, Novel method for measurement of granular temperature distributions in two-dimensional vibro-fluidised beds, Powder Technol. **113**, 14 (2000).

[41] J. R. Royer, D. J. Evans, L. Oyarte, Q. Guo, E. Kapit, M. E. Möbius, S. R. Waitukaitis, and H. M. Jaeger, High-speed tracking of rupture and clustering in freely falling granular streams, Nature **459**, 1110 (2009).

[42] N. Lardier, P. Roudier, B. Clothier, and G. R. Willmott, High-speed photography of water drop impacts on sand and soil, Eur. J. Soil. Sci. **70**, 245 (2019).

[43] J. Hlosta, D. Žurovec, J. Rozbroj, Á. Ramírez-Gómez, J. Nečas, and J. Zegzulka, Experimental determination of particle-particle restitution coefficient via double pendulum method, Chem. Eng. Res. Des. **135**, 222 (2018).

[44] Q. H. Zhang, S. Y. Wang, H. L. Lu, Q. J. Wang, M. Tao, and G. D. Liu, Impact velocity-dependent restitution coefficient using a coupled Eulerian fluid phase-Eulerian solid phase-Lagrangian discrete particles phase model in gas-monodisperse particles internally circulating fluidized bed, Int. J. Multiphas. Flow **105**, 142 (2018).

[45] Y. F. Duan and Z. G. Feng, Incorporation of velocity-dependent restitution coefficient and particle surface friction into kinetic theory for modeling granular flow cooling, Phys. Rev. E **96**, 062907 (2017).

[46] Y. Grasselli, G. Bossis, and G. Goutallier, Velocity-dependent restitution coefficient and granular cooling in microgravity, Euro. Phys. Lett. **86**, 60007 (2009).